CHIN. PHYS. LETT. Vol. 34, No. 1 (2017) 013401

Measurement of the Low-Energy Rb^+–Rb Total Collision Rate in an Ion-Neutral Hybrid Trap *

Shuang-Fei Lv(吕双飞)[1], Feng-Dong Jia(贾凤东)[1], Jin-Yun Liu(刘晋允)[1], Xiang-Yuan Xu(许祥源)[2,3], Ping Xue(薛平)[2**], Zhi-Ping Zhong(钟志萍)[1**]

[1]*School of Physical Sciences, University of Chinese Academy of Sciences, Beijing 100049*
[2]*State Key Laboratory of Low-Dimensional Quantum Physics, Department of Physics, Tsinghua University, and Collaborative Innovation Center of Quantum Matter, Beijing 100084*
[3]*Department of Physics, Capital Normal University, Beijing 100037*

(Received 1 September 2016)

An ion–neutral hybrid trap is built to study low-energy ion–atom collisions. The ion–neutral hybrid trap is combined with two spatially concentric traps: a linear Paul trap for the ionic species and a magneto-optical trap (MOT) for the neutral species. The total ion–atom collision rate coefficient k_{ia} between ^{87}Rb atoms and optically dark $^{87}Rb^+$ ions is measured by monitoring the reduction of the steady-state MOT atoms by sequentially introducing various mechanisms, namely photoionization and ion–atom collisions. In contrast to other experiments, a concise experimental procedure is devised to obtain the loss rates of the MOT atoms due to photoionization and ion–atom collisions in one experimental cycle, and then the collision rate k_{ia} of cold ^{87}Rb atoms with $^{87}Rb^+$ ions is deduced to $0.94(\pm0.24)\times10^{-13}\ m^3/s$ with $T_i = 3770(\pm100)\ K$ measured by the time of flight of the ion signal. The measurements show good agreement with the collision rate derived from the Langevin model.

PACS: 34.50.Cx, 34.80.Dp, 34.90.+q DOI: 10.1088/0256-307X/34/1/013401

Cold ion–neutral collisions are different from neutral–neutral[1–3] and ion–ion collisions, and are rarely studied in the low-energy range.[4] The long range ion–atom potential can be described by $-C_4/r$, where $C_4 = \alpha e^2/(8\pi\varepsilon_0)$, with α being the static electric polarizability of the atom and r the ion–atom separation. The scattering mediated by this potential is the primary channel for the exchange of energy between the ions and atoms. Therefore, the investigations of ion–neutral collisions at low energy are very useful for the study of sympathetic cooling[5–7] of atomic ion translational motion[8,9] and molecular ions' internal degrees of freedom,[10] especially for the optically dark species that are not amenable to direct laser cooling.[4,9]

An ion–neutral hybrid trap is a combination of two separate but spatially concentric traps, usually a magneto-optical trap (MOT) for the neutral species and a mass-selective linear Paul trap for the ionic species.[8] Over the past decade, since the hybrid trap was originally proposed,[5] both experimental[4,6,9,11–17] and theoretical[7,18–21] interest in low-energy ion–neutral collisions has surged. Hybrid traps also make excellent cold-chemistry laboratories, and they can, for example, provide additional control for accessing and manipulating chemical reaction rates.[22–24]

Several methods have been used to measure scattering rates using a hybrid trap, including monitoring the neutral atom fluorescence decay from an optical dipole trap(ODT)[12,22] or measuring the ion fluorescence decay from a Paul trap.[10,25] Recently, hybrid trap measurements of the total elastic and charge-exchange collision rates for closed-shell, optically dark $^{85}Rb^+$ ions with the ion temperature $T_i \approx 1000$ K and Na^+ ions with $T_i \approx 140$ or 1070 K were reported,[15,26] and note that T_i is acquired by SIMION simulation. In Refs. [15,26], the changing of the fluorescence of the neutral species is monitored when introducing photoionization (PI) and ion–atom (ia) collisions, and then the fluorescence change is used to determine the total collision rate of ion–atom collisions.

In this work, an ion–neutral hybrid trap is built following Ref. [4]. We devise a concise experimental procedure to obtain both the loss rates of the MOT atoms due to photoionization and ion–atom collisions in one experimental cycle, and then deduce the total elastic and resonant charge-exchange ion–atom collision rate coefficient k_{ia} of cold ^{87}Rb atoms with optically dark $^{87}Rb^+$ ions. In addition, the ion temperature is determined to be $T_i = 3770(\pm100)$ K by directly measuring the ion arrival time-of-flight distribution.

Figure 1 is the schematic diagram of our ion–atom hybrid trap and the two-photon ionization scheme of ^{87}Rb. The MOT is constructed mainly by a gradient magnetic field (not shown in Fig. 1) and three pairs of cooling/trapping and repumping beams (illustrated in red), and the MOT locates at the intersection point represented by the red sphere. The total number and the temperature of the cold atoms are directly measured by the time-of-flight (TOF) method.[27] The MOT fluorescence is detected by a homemade photodetector and calibrated by TOF, and then the cold atom number can be obtained in real time. To improve the signal-to-noise ratio of the fluorescence measurements, a narrow bandpass filter centered at 780 nm

*Supported by the National Natural Science Foundation of China under Grant Nos 11604334, 61227807 and 61575108, and the Tsinghua Initiative Scientific Research Program under Grant No 2013THZ02-3, and the Beijing Natural Science Foundation under Grant No 1164016.

**Corresponding author. Email: zpzhong@ucas.ac.cn; xuep@tsinghua.edu.cn

© 2017 Chinese Physical Society and IOP Publishing Ltd

with a full width at half maximum of ±2 nm is placed in front of the photodetector. The typical parameters of the MOT are as follows: the total intensity of the cooling/trapping beams is approximately 70 mW with a diameter of 10 mm, the intensity of the repumping beams is approximately 10 mW, and the gradient magnetic field is approximately 10 G/cm. As a result, about as many as $N_a = 6.04(\pm 0.33) \times 10^6$ ^{87}Rb atoms can be trapped, and the $1/e$ half waist of the cold atomic cloud is measured to be approximately 0.3 mm.

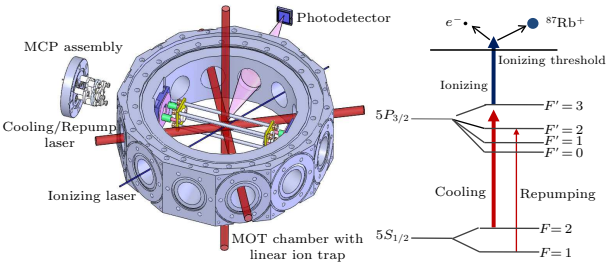

Fig. 1. Schematic diagram of our ion-neutral hybrid trap (left) and the two-photon ionization scheme of ^{87}Rb (right) in this work. The MOT and linear Paul trap are overlapped as shown, with the cooling lasers illustrated in red, and the MOT located at the intersection point represented by the red sphere. The ionizing laser beam is illustrated in blue. The microchannel plate (MCP) is used to detect the trapped ions by appropriately switching off the voltage on the hollow end-cap electrode closer to the MCP. The MOT fluorescence is detected by a homemade photodetector. To improve the signal-to-noise ratio of the fluorescence measurements, a narrow bandpass filter centered at 780 nm with a full width at half maximum of ±2 nm is placed in front of the photodetector.

The linear Paul trap is comprised of four rf central parallel rods arranged in a quadrupole configuration and two dc hollow end-cap ring electrodes along the cylindrical axis, as shown in Fig. 1. The rod diameter is approximately 3 mm and the separation of the neighboring quadrupole electrodes is approximately 15 mm. An rf voltage is applied to diagonally opposite rods, with the voltage along the two diagonals being 180° out of phase,[4] providing trapping in the transverse dimension.[27] The axial confinement is established by a static voltage V_{end} applied to the end-cap ring electrodes. The typical parameters of the linear Paul trap are as follows: the applied rf amplitude and frequency are 120 V and 500 kHz, respectively, and $V_{end} = 200$ V, which results in an ion trap depth of approximately 0.7 eV and axial and radial trap frequencies 95 and 10 kHz, respectively. Most importantly, the MOT and the linear Paul trap are spatially overlapped, as shown on the left-hand side of Fig. 1. The ions are produced by two-photon ionization of cold atoms trapped in the MOT, as shown on the right-hand side of Fig. 1. A microchannel plate (MCP) is used to detect the trapped ions by appropriately switching off the voltage on the end-cap ring electrode closer to the MCP.

The behavior of the MCP gain as a function of the voltage applied to the MCP was tested at a fixed ion input current. Figure 2 shows a well-defined linear logarithmic relation between the output ion signal (which is proportional to the gain) and the voltage applied to the MCP, indicating that the MCP is not saturated. In the experiments described here, we apply a high dc voltage of $U_{MCP} = 1620$ V on the MCP. The black triangle shown in the inset is the typical ion TOF signal detected by the MCP, and we can deduce the temperature of the ion cloud $T_i = 3770(\pm 100)$ K by fitting the TOF signal with a Maxwell–Boltzmann distribution, shown by the red line.

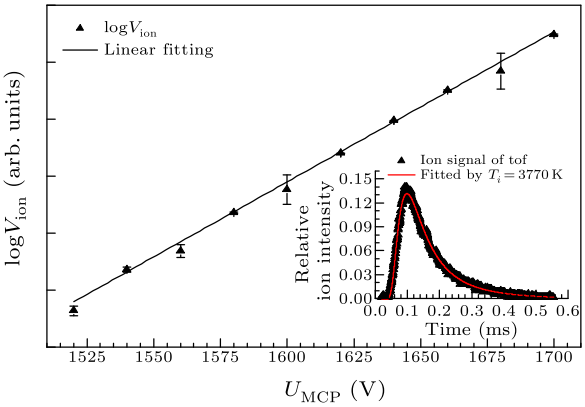

Fig. 2. The test of deviation from the expected exponential behavior of the MCP gain as a function of the voltage applied to the MCP at a fixed ion input current. The inset is the typical ion TOF signal shown in the black triangle and the fitting of the TOF signal is shown in red.

The rate-equation model is used to describe the evolution of the MOT atom number due to ionization and ion–atom collisions, and a concise experimental procedure is devised to determine the loss rate. As is well known, the time dependence of N_a in an MOT can be written as[28]

$$\frac{dN_a}{dt} = L - \gamma_x N_a, \tag{1}$$

where L is the loading rate of the atoms from the background vapor into the MOT, and γ_x is the loss rate of the MOT atoms. Here γ_x can be obtained due to different mechanisms, such as collisions between cold atoms, photoionization of cold atoms, and ion–atom collisions. The time-dependent solution of Eq. (1) under an initial condition $N_a(0) = 0$ can be written as

$$N_a(t) = N_a^0(1 - e^{-\gamma_x t}), \tag{2}$$

where $N_a^0 = L/\gamma_x$ is the steady-state atom number in the MOT with $t \to \infty$.

The collision-rate coefficient between Rb and optically dark Rb^+ is measured by monitoring the reduction of the steady-state MOT atoms by sequentially introducing various mechanisms, namely photoionization and ion–atom collisions. We devise a concise experimental procedure to obtain both the loss rates of the MOT atoms due to PI and ion–atom interactions in one experimental cycle as shown in Fig. 3. In detail, there are three steps in one experimental cycle. In the first step, from 0 to T_1, an MOT is loaded for as long as 40 s until saturation. In this step, one can obtain the loading rate L, the loss rate of the

MOT atoms $\gamma_{\rm MOT}$ and the steady-state atom number $N_0 = \frac{L}{\gamma_{\rm MOT}}$. In the second step, from T_1 to T_2, a blue diode continuous-wave laser at 473 nm is introduced to photoionize the excited MOT atoms, for a duration as long as 30 s to reach a new atom fluorescence steady state. Here the steady number of cold atoms can be expressed as $N_{\rm t} = \frac{L}{\gamma_{\rm t}}$ with $\gamma_{\rm t} = \gamma_{\rm PI} + \gamma_{\rm MOT}$, therefore one can obtain $\gamma_{\rm PI} = \gamma_{\rm t} - \gamma_{\rm MOT}$ in this step. In the third step, both the blue laser and ion trap are turned on, the ions are accumulated in the ion trap and enhance the ion–atom collisions. After 30 s the new steady-state number of cold atoms, $N_{\rm total} = \frac{L}{\gamma_{\rm tot}}$ with $\gamma_{\rm tot} = \gamma_{\rm ia} + \gamma_{\rm PI} + \gamma_{\rm MOT}$, is reached, and finally we can obtain $\gamma_{\rm ia} = \gamma_{\rm tot} - \gamma_{\rm t}$ in one experimental cycle.

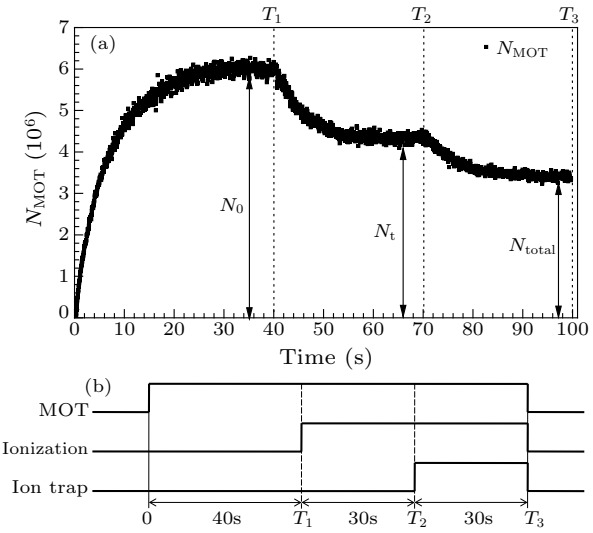

Fig. 3. Temporal sequence for one experimental cycle and the corresponding experimental MOT fluorescence. From 0 to T_1 the MOT is loaded for 40 s to saturation, where it contains $\approx 6.04(\pm0.33) \times 10^6$ atoms. From T_1 to T_2, the photoionization laser is switched on. From T_2 to T_3, both the blue photoionization laser and ion trap are switched on.

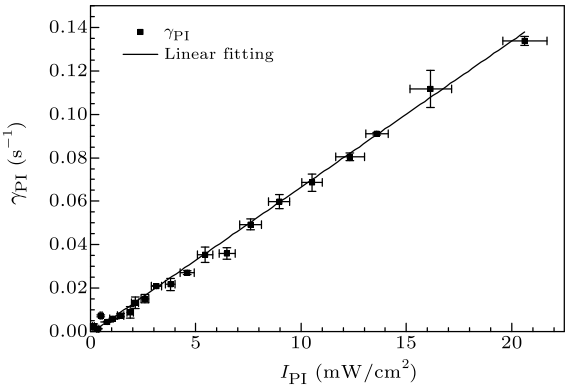

Fig. 4. Loss rate $\gamma_{\rm PI}$ due to photoionization as a function of the ionizing laser intensity $I_{\rm PI}$ and linear fitting.

Figure 4 shows a well-defined linear relation between $\gamma_{\rm PI}$ and the ionizing laser intensity $I_{\rm PI}$, which means that $I_{\rm PI}$ is far from saturation and ensures that we can use Eq. (2) to deduce various loss rates. Here $\gamma_{\rm PI}$ can be fitted by

$$\gamma_{\rm PI} = \zeta I_{\rm PI}, \tag{3}$$

where $\zeta = \frac{\sigma_{\rm PI}\lambda_{\rm PI} f_{\rm e}}{hc}$, with $f_{\rm e}$ being the fraction of atoms in the excited state. We directly obtain $\zeta = 0.00672(\pm0.00012)\,{\rm m}^2/{\rm J}$ according to the experimental data from Fig. 4.

Figure 5 shows the relationship between $\gamma_{\rm ia}$ and the ionizing laser intensity $I_{\rm PI}$, which can be described by[15]

$$\gamma_{\rm ia} = \frac{N_{\rm i}^0 k_{\rm ia}}{V_{\rm IT}}(1 - e^{-\kappa I_{\rm PI}}), \tag{4}$$

where $k_{\rm ia}$ is the ion–atom collision rate coefficient, $V_{\rm IT}$ is the ion-trapping volume to be discussed later, and κ is the intensity-loss coefficient with units of inverse intensity due to the finite potential depth of the ion trap. Here $\kappa = 0.654(\pm0.088)\,{\rm m}^2/{\rm W}$ is determined by fitting the experimental data in Fig. 5 with Eq. (4). The maximum trapped ion number $N_{\rm i}^0$ is then expressed as[12]

$$N_{\rm i}^0 = N_{\rm a}\zeta\frac{1}{\gamma_{\rm ia}\kappa}. \tag{5}$$

In our case, we can easily calculate that $N_{\rm i}^0 = 1.13(\pm0.16) \times 10^6$ with $N_{\rm a} = 6.04(\pm0.33) \times 10^6$, $\zeta = 0.00672(\pm0.00012)\,{\rm m}^2/{\rm J}$, $\gamma_{\rm ia} = 0.067(\pm0.010)$, and $\kappa = 0.654(\pm0.088)\,{\rm m}^2/{\rm W}$.

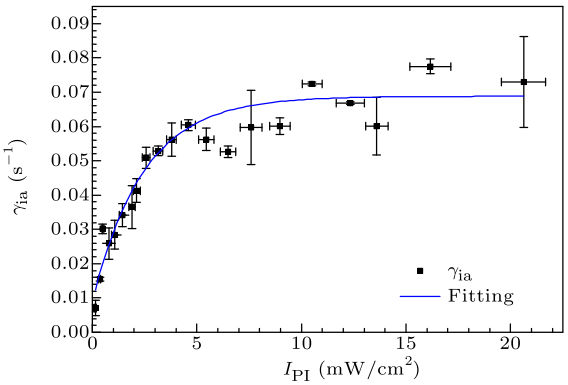

Fig. 5. Loss rate $\gamma_{\rm ia}$ due to ion–atom collisions as a function of the ionizing laser intensity $I_{\rm PI}$ and fitted by Eq. (4).

To determine $k_{\rm ia}$, the last parameter in Eq. (4) is the dark Rb^+ ion cloud volume $V_{\rm IT}$. We use the MOT to probe the dark ion cloud by translating it across the saturated ion cloud along one transverse dimension with a magnetic bias field.[26] We measured $\gamma_{\rm ia}/N_{\rm i}$ as a function of cold atom positions, as shown in Fig. 6, and the changing concentricity function follows the equation as[26]

$$C = e^{-(x_{0,1}^2 + x_{0,2}^2)/(r_{\rm a}^2 + r_{\rm I}^2)} e^{-x_{0,3}^2/(r_{\rm a}^2 + r_{\rm I,3}^2)}, \tag{6}$$

where $r_{\rm a}$ is the radius of the cold atom cloud, and $r_{\rm I,1}$, $r_{\rm I,2}$ and $r_{\rm I,3}$ are the radial directions x, y and axial direction z of the ion cloud, respectively, $\gamma_{\rm ia}/N_{\rm I}$ should be proportional to C.[26] By fitting $\gamma_{\rm ia}/N_{\rm I}$ with the relative MOT center position, we can deduce that the radius of the ion cloud is $r_{\rm I,1} = r_{\rm I,2} = 2.7(\pm0.1)$ mm. According to the ratio of axial trap frequency to radial trap frequency, which is approximately 9.5:1, we can estimate the axial radius as $r_{\rm I,3} = 25.2(\pm0.8)$ mm.

The volume of the ion cloud is then deduced approximately to be $V_{\rm IT} = 1.58(\pm0.24) \times 10^{-7}\,{\rm m}^3$ in our case. Finally, the ion–atom collision rate $k_{\rm ia} = 0.94(\pm0.24) \times 10^{-13}\,{\rm m}^3/{\rm s}$ is obtained, as listed in Table 1, as well as some key values used in the determination of $k_{\rm ia}$.

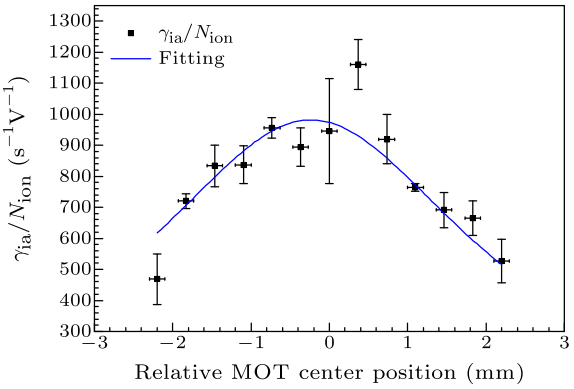

Fig. 6. Loss rate $\gamma_{\rm ia}$ normalized by the steady-state ion intensity as a function of the center position of a smaller MOT relative to the geometric center of the ion trap along the transverse dimension.

Table 1. Values of relative parameters used in determination of $k_{\rm ia}$.

Parameter	Value	Units
N_a	$6.04(\pm0.33) \times 10^6$	
ζ	$0.00672(\pm0.00012)$	$\rm m^2J^{-1}$
$\gamma_{\rm ia}$	$0.067(\pm0.010)$	$\rm s^{-1}$
κ	$0.654(\pm0.088)$	$\rm m^2W^{-1}$
$N_{\rm i}^0$	$1.13(\pm0.16) \times 10^6$	
$V_{\rm IT}$	$1.58(\pm0.24) \times 10^{-7}$	$\rm m^3$
$k_{\rm ia}$	$0.94(\pm0.24) \times 10^{-13}$	$\rm m^3s^{-1}$

We estimate the collision-rate coefficient based on the classical Langevin model with $T_{\rm i} \approx 3770\,{\rm K}$ directly measured by the time-of-flight of the ion signal. The total cross section σ consists of the elastic and charge-exchange cross sections, $\sigma_{\rm el}$ and $\sigma_{\rm ec}$. However, in the collision energy range in our experiment, $\sigma_{\rm el} \gg \sigma_{\rm ec}$, thus the total cross section $\sigma \approx \sigma_{\rm el}$, which can be expressed as

$$\sigma \approx \sigma_{\rm ec} \approx 5.08\Big(\frac{\mu C_4^2}{\hbar^2}\Big)^{1/3} E_{\rm col}^{-1/3}, \qquad (7)$$

where $C_4 = \alpha e^2/(8\pi\varepsilon_0)$, and α is the static dipole polarization of the neutral atoms in the ground states. For Rb, $\alpha \approx 47 \times 10^{-30}\,{\rm m}^3$, and $C_4 \approx 5.26 \times 10^{-39}\,{\rm C\cdot m^2/V}$. Assuming that the ion speeds follow the Maxwell–Boltzman distribution $f(v)$, we can then compute the theoretical collision rate coefficient as $k_{\rm ia} = \int \sigma f(v) v dv = \langle \sigma v \rangle = 0.69 \times 10^{-13}\,{\rm m}^3/{\rm s}$ for the Rb atoms in the ground state. However, in our experiment, the ratio of atom number in the ground and the excited states is approximately 0.76:0.24, and accordingly the ratio of polarizability is approximately 1:2.7. Eventually, the theoretical collision rate coefficient should be revised as $k_{\rm ia} = 0.86 \times 10^{-13}\,{\rm m}^3/{\rm s}$ which agrees well with the experimental data of $0.94(\pm0.24) \times 10^{-13}\,{\rm m}^3/{\rm s}$.

In summary, we have built an ion-neutral hybrid trap, in which the total elastic and resonant charge-exchange ion–atom collision rate coefficient $k_{\rm ia} = 0.94(\pm0.24) \times 10^{-13}\,{\rm m}^3/{\rm s}$ of cold Rb with optically dark $^{87}{\rm Rb}^+$ ions is measured by a concise experimental procedure. The results agree well with a simple calculation considered as the classical Langevin formula of the cross-section and the ion–atom collision energy $T_{\rm i} = 3770(\pm100)\,{\rm K}$. In the future, our ion–neutral hybrid trap will facilitate the systematic study of ion–atom collisions and chemical reactions in the wide energy region, including interesting phenomena such as sympathetic cooling, and production of ultracold molecular ions.

References

[1] Zhang J C, Zhu Z L, Liu Y F and Sun J F 2011 *Chin. Phys. Lett.* **28** 123401
[2] Zhang J C, Zhu Z L, Liu Y F and Sun J F 2013 *Chin. Phys. Lett.* **30** 023401
[3] Zhang J C, Zhu Z L and Sun J F 2012 *Acta Phys. Sin.* **9** 093401 (in Chinese)
[4] Ravi K, Lee S, Sharma A, Werth G and Rangwala S A 2012 *Nat. Commun.* **3** 1126
[5] Smith W W, Makarov O P and Lin J 2005 *J. Mod. Opt.* **52** 2253
[6] Goodman D S, Sivarajah I, Wells J E, Narducci F A and Smith W W 2012 *Phys. Rev.* A **86** 033408
[7] Hudson E R 2009 *Phys. Rev.* A **79** 032716
[8] Deiglmayr J, Göritz A, Best T, Weidemüller M and Wester R 2012 *Phys. Rev.* A **86** 043438
[9] Sivarajah I, Goodman D S, Wells J E, Narducci F A and Smith W W 2012 *Phys. Rev.* A **86** 063419
[10] Rellergert W G, Sullivan S T, Schowalter S J, Kotochigova S, Chen K and Hudson E R 2013 *Nature* **495** 490
[11] Hall F H J, Aymar M, Bouloufa-Maafa N, Dulieu O and Willitsch S 2011 *Phys. Rev. Lett.* **107** 243202
[12] Haze S, Hata S, Fujinaga M and Mukaiyama T 2013 *Phys. Rev.* A **87** 052715
[13] Rellergert W G, Sullivan S T, Kotochigova S, Petrov A, Chen K, Schowalter S J and Hudson E R 2011 *Phys. Rev. Lett.* **107** 243201
[14] Sullivan S T, Rellergert W G, Kotochigova S and Hudson E R 2012 *Phys. Rev. Lett.* **109** 223002
[15] Lee S, Ravi K and Rangwala S A 2013 *Phys. Rev.* A **87** 052701
[16] Chen K, Sullivan S T and Hudson E R 2014 *Phys. Rev. Lett.* **112** 143009
[17] Cetina M, Grier A T and Vuletic V 2012 *Phys. Rev. Lett.* **109** 253201
[18] Côte R and Dalgarno A 2000 *Phys. Rev.* A **62** 012709
[19] Makarov O P, Côte R, Michels H and Smith W W 2003 *Phys. Rev.* A **67** 042705
[20] Zhang P, Dalgarno A and Côte R 2009 *Phys. Rev.* A **80** 030703
[21] Li M and Gao B 2012 *Phys. Rev.* A **86** 012707
[22] Schmid S, Härter A, Frisch A, Hoinka S and Denschlag J H 2012 *Rev. Sci. Instrum.* **83** 053108
[23] Hall F H, Eberle P, Hegi G, Raoult M, Aymar M, Dulieu O and Willitsch S 2013 *Mol. Phys.* **111** 2020
[24] Tomza M 2015 *Phys. Rev. Lett.* **115** 063201
[25] Grier A T, Cetina M, Oručević F and Vuletić V 2009 *Phys. Rev. Lett.* **102** 223201
[26] Goodman D S, Wells J E, Kwolek J M, Bluümel R, Narducci F A and Smith W W 2015 *Phys. Rev.* A **91** 012709
[27] Paul W 1990 *Rev. Mod. Phys.* **62** 531
[28] Cooper C J, Hillenbrand G, Rink J, Townsend C G, Zetie K and Foot C J 1994 *Europhys. Lett.* **28** 397